International Journal of Pavement Engineering

ISSN: (Print) (Online) Journal homepage: https://www.tandfonline.com/loi/gpav20

Measurement of pavement rutting trajectories on two-lane highway using the 3D line scanning laser system

Wenting Luo, Yong Qin, Dejin Zhang & Lin Li

To cite this article: Wenting Luo, Yong Qin, Dejin Zhang & Lin Li (2022): Measurement of pavement rutting trajectories on two-lane highway using the 3D line scanning laser system, International Journal of Pavement Engineering, DOI: 10.1080/10298436.2022.2149753

To link to this article: https://doi.org/10.1080/10298436.2022.2149753

Published online: 16 Dec 2022.

https://doi.org/10.1080/10298436.2022.2149753

Taylor & Francis
Taylor & Francis Group

Measurement of pavement rutting trajectories on two-lane highway using the 3D line scanning laser system

Wenting Luo [a], Yong Qin [b], Dejin Zhang [c] and Lin Li [a]

[a]College of Transportation Engineering, Nanjing Tech University, Nanjing, People's Republic of China; [b]The State Key Laboratory of Rail Traffic Control and Safety, Beijing Jiaotong University, Beijing, People's Republic of China; [c]School of Architecture and Urban Planning, Shenzhen University, Shenzhen, People's Republic of China

ABSTRACT
Lane departure is one of the important reasons for traffic accidents on a two-lane highway. However, the vehicles' trajectories obtained by the traditional methods only represent wheel wandering in specifical situations, but do not reflect a regular pattern of lane departure. Pavement rutting trajectories are applied to investigate the regular pattern of lane departure in this paper. A 3D line scanning laser system is utilized to obtain 3D deformed pavement surface images, and rutting trajectories are measured based on the collected data. Inertial Measurement Unit and Distance Measuring Instrument are used to describe lane centreline trajectory of two-lane highways, and curve radius and curve length are measured. A test site on a two-lane highway is chosen as the test bed. Based on the field data, the impacts of undivided opposite lanes, curve turning direction, geometric features, curve radius and curve length on lane departure are analyzed, and the hazardous locations with large lane departures are identified. The significance of this study is that it provides a method to describe a regular pattern of lane departure on two-lane highways, and also benefits transportation agencies in traffic safety analysis and the horizontal alignment design of two-lane highways.

ARTICLE HISTORY
Received 14 July 2022
Accepted 15 November 2022

KEYWORDS
Two-lane highways; lane departure; horizontal alignment; pavement rutting; inertial measurement unit (IMU); 3D line scanning laser system

1. Introduction

A disproportionate number of serious crashes occur on two-lane highways although they only represent a fraction of the roadway network (Hanley and Forkenbrock 2005). Lane departure is one of the important reasons for traffic accidents on two-lane highways (Gungor and Al-Qadi 2022, Saleh 2020). Based on previous research, the performance of vehicles, climate, driver behaviour and road alignments are the important elements possibly causing wheel wandering (Siddharthan *et al.*2017, Zhou *et al.* 2019). Among them, the performance of vehicles, climate and driver behaviour are the elements with random variation. Horizontal alignments of two-lane highways including curve radius and curve length also affect lane departure, which are unchanged since the completion of the roads Luo and Li (2018). The key point of lane departure pattern detection is describing the vehicles' trajectories under various situations which include changed and unchanged intervening factors (Yeganeh *et al.* 2021, Yeganeh *et al.* 2022). Pavement ruts are formed based on 'repeated traffic loads' (Zhao *et al.* 2020, Ekblad *et al.* 2021). The 'repeated traffic loads' represent 'various vehicles' and 'long time'. The 'various vehicles' cover various vehicle types and various driver behaviours; and the 'long time' covers various climates (Saleeb *et al.* 2005, Luo *et al.* 2020). Therefore, rutting trajectories are applied to investigate the regular pattern of lane departure in this study. Analysis of the impacts of horizontal alignments on lane departure benefits for geometry design of two-lane highways, so this study aims to find out the relationship between horizontal alignments and lane departure.

The widely used methods for road alignment measurement include the satellite imagery-based method, vision-based method and Mobile Mapping System (MMS)-based method. Satellite imagery provides a digital map for horizontal alignment data extraction, which is low-cost in data collection and has a data source of a complete roadway network (Bento *et al.* 2019). A number of algorithms are developed for horizontal alignment surveys based on satellite imaging data, such as Curve Calculator, Curvature Extension and Curve Finder (Rasdorf *et al.* 2012). However, these methods did not archive automatic PC/PT station detection. A number of vision-based roadway alignment measuring methods were presented in previous studies (Ishikawa *et al.* 2007, Choi and Lee 2006, Tsai *et al.* 2010). The vision-based methods measure horizontal alignments using front-view pictures, which are not suitable for continuous measurement. Mobile Mapping System is incorporated with Global Positioning System (GPS), Inertial Measurement Unit (IMU) and Distance Measuring Instrument (DMI) (Luo *et al.* 2018). The survey vehicles' trajectory along the roadway collected by MMS is considered as lane centreline for horizontal alignment measurement (Findley *et al.* 2011, Ai and Tsai 2014, Ben-Arieh *et al.* 2004, Imran *et al.* 2006). However, the lane offset of the survey vehicle reduces the accuracy of horizontal alignment measurement.

CONTACT Lin Li 18805915372@163.com

Unmanned Aerial Vehicle (UAV) and vehicle positioning system are widely used to acquire vehicles' trajectories (Kim *et al.* 2018). Due to the battery power supplied mode and the capture range of UAV, the number of monitored vehicles and the time of data collection are limited (Outay *et al.* 2020). Therefore, the data collected by UAV cannot be used to represent the regular pattern of lane departure. Global Positioning System (GPS) is another method to collect vehicles' trajectories. The resolution of GPS positioning is around 1 m, which is widely used in traffic flow analysis but not suitable for lane departure detection.

The trajectories of pavement ruts are used to detect the regular pattern of lane departure on two-lane highways in this study. There were a lot of methods for pavement rutting measurement. A multi-point laser system and line scanning laser system are the widely used equipment for pavement rutting measurement (Hong *et al.* 2018, Zhang *et al.* 2018) The multi-point laser system is mounted in front of or on the rear of survey vehicle Hui *et al.* (2018). The several-point lasers on a multi-point laser system measure the distance from the lasers to the pavement, and the rutting shape is described based on the collected data on specific positions Luo *et al.* (2019). Different from the multi-point laser system, the line scanning laser system involves more than 1000-point lasers, which, in essence, represents a continuous profile with entire lane coverage (Qiu *et al.* 2018, Zhang *et al.* 2018, Ding *et al.* 2022). The line scanning laser system has a higher resolution than the multi-point laser system for rutting measurement Hong *et al.* 2018.

Transportation agencies need accurate data inventory containing lane departure trajectory to implement two-lane highway safety analysis. The vehicles' trajectories measured by traditional methods can not represent the regular pattern of lane departure on two-lane highways. This study provides a novel method to detect the regular pattern of lane departure based on pavement rutting trajectories. The contributions of this study are as follows:

The on-board measurements of horizontal alignments is safer, more accurate and more efficient than the widely used manual measurements.

Rutting measurement using a 3D line scanning laser extracts more information (such as rutting trajectories) than the measurement using a point laser.

It proposes a precise, novel and objective method for investigating the regular pattern of lane departure on two-lane highways based on pavement rutting trajectories, which is a benefit for transportation agencies doing traffic safety analysis and horizontal alignment design.

2. Proposed Solution

Lane departure is a danger for two-lane highways due to the high speed and the undivided lanes in opposing directions. This study attempts to describe the vehicles' trajectories via pavement rutting trajectories. Based on the analysis of the impacts of horizontal alignments, the lane departure of two-lane highways is detected. The flow chart of the study is shown in Figure 1.

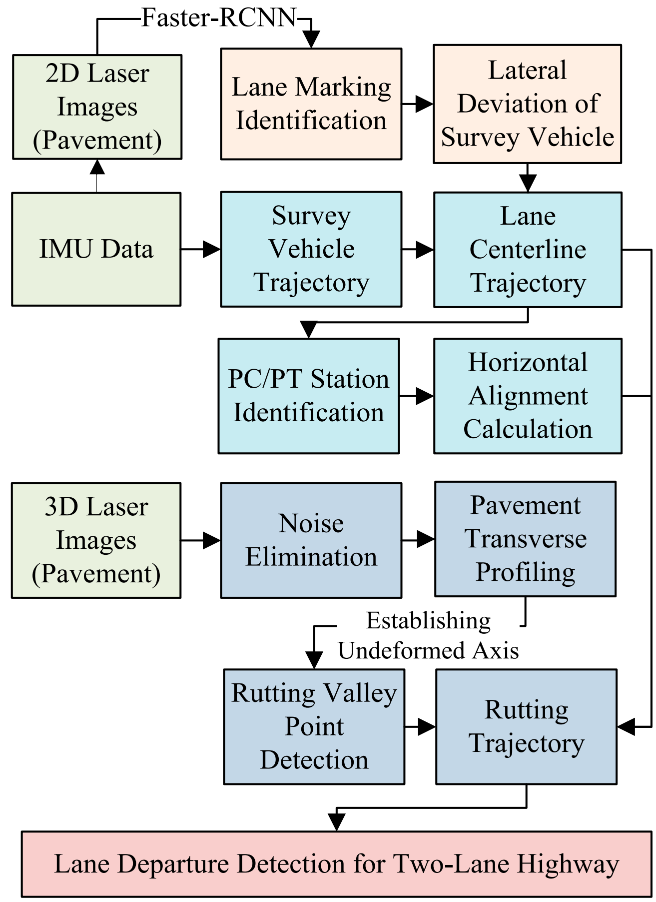

Figure 1. The flow chart of proposed solutions.

2.1. Data preparation

Three types of data are the data source in this study. The 2D and 3D pavement laser images are collected by a 3D line scanning laser system, which is used for rutting measurement. The heading angles data are collected by the Inertial Measurement Unit (IMU), which is applied for horizontal alignment measurement.

2.2 Characterisation measurement of the pavement

An automatic method for horizontal alignments and rutting trajectories measurement is proposed in this study. A Faster R-CNN model is applied to detect the lane markings on 2D pavement images. Based on the detected lane markings the lane offset of the survey vehicle is determined. Subsequently, the k-mean clustering method is applied to detect PC/PT stations, and the chord offset method is used to calculate the curve radius. To measure the rutting trajectories, the undeformed horizontal axis is established and utilised for rutting valley point detection; and rutting trajectories are determined by referring to the locations of lane markings and the valley points of ruts.

2.3. Lane departure detection

A road section of two-lane highways is selected as the test bed. The lane departure is measured in a field based on rutting trajectories. Referring to the field data, the impacts of undivided lanes in opposing directions, turning direction of curves, geometric features, curve radius and curve length on lane departure are evaluated. Indeed, hazardous sections with lane departure on two-lane highways are detected.

3. Data acquisition system

The Digital Highway Data Vehicle (DHDV) developed by WayLink Systems Corporation with collaborations from Oklahoma State University is applied to acquire full lane information for horizontal alignments and rutting trajectories measurement in this study. The 3D line scanning laser system and Inertial Measurement Unit (IMU) are integrated and synchronised into DHDV, and the data collection speed of DHDV on roadways is up to 100 km/h. The exterior and interior appearances of DHDV are shown in Figure 2.

Two 3D line scanning laser systems mounted on DHDV are composed of eight high-resolution cameras and two sets of lasers, as shown in Figure 2 (Li *et al.* 2018). The 3D line scanning laser system acquires fully matched 2D and 3D laser images at the same time. The line scanning laser light with a fixed wavelength is the only light source for the cameras, so the laser images are shadow-free whether collected day or night time Bosurgi *et al.*(2022). A laser image with 4096 × 2048 pixels covers a full-lane (4 m) width and 2 m in length. The vertical resolution of the 3D laser image is 0.3 mm, and the longitudinal and transverse resolution is 1 mm. The resolution of the 2D laser image is 1 mm.

Inertial Measuring Unit (IMU) is a self-contained sensor consisting of accelerometers and fibre-optic gyroscopes. The IMU mounted on the interior floor between the two axes of the survey vehicle's chassis measures Euler angles, which are termed a roll (Euler angle about the x-axis), pitch (Euler angle about the y-axis) and yaw (Euler angle about the z-axis). The measured Euler angles coincide with the body roll angle of the survey vehicle.

4. Methdology

4.1. Trajectory extraction of pavement centreline

The trajectory of the pavement centreline is applied to measure roadway alignments. First, the trajectory of DHDV along the roadway is extracted. Second, by referring to the image positions of lane markings, the trajectory of DHDV on a lane is determined. Finally, based on the distance from the road centre to DHDV the trajectory of the pavement centreline is obtained. The details are shown as follows.

4.1.1 Pavement lane marking identification

Normally lane markings are presented as white or orange colour, while the pavement is presented as black colour. In this study lane markings are identified based on their colour on 2D laser images. Through years of research, many segmentation methods based on neural networks have been developed. Region-based Convolutional Neural Network (R-CNN) is the first object detection algorithm based on deep learning Zhai *et al.*(2021) However, feature extraction by serial and selective search wastes lots of computing time. Fast R-CNN shortens the time used for feature extraction by serial, but the algorithm of selective search still exists Deng *et al.*(2017). Faster R-CNN developed in 2015 is an improvement of Fast R-CNN Gao *et al.*(2021). In the model the selective search is replaced by a Region Proposal Network (RPN), so its efficiency is significantly improved Zhang *et al.*(2018).

The Faster R-CNN model is applied for lane marking identification in this study. The examples of lane marking identification based on the Faster R-CNN model are shown in Figure 3. Herein, the green bounding box with lane marking label is the ground-truth lane marking box, and the blue bounding box with classification confidence score is the predicted result. The blue bounding boxes almost overlap the green bounding box in Figure 3. The performance of Faster R-CNN is evaluated by the PR curve method. According to

Figure 2. The interior and exterior of DHDV.

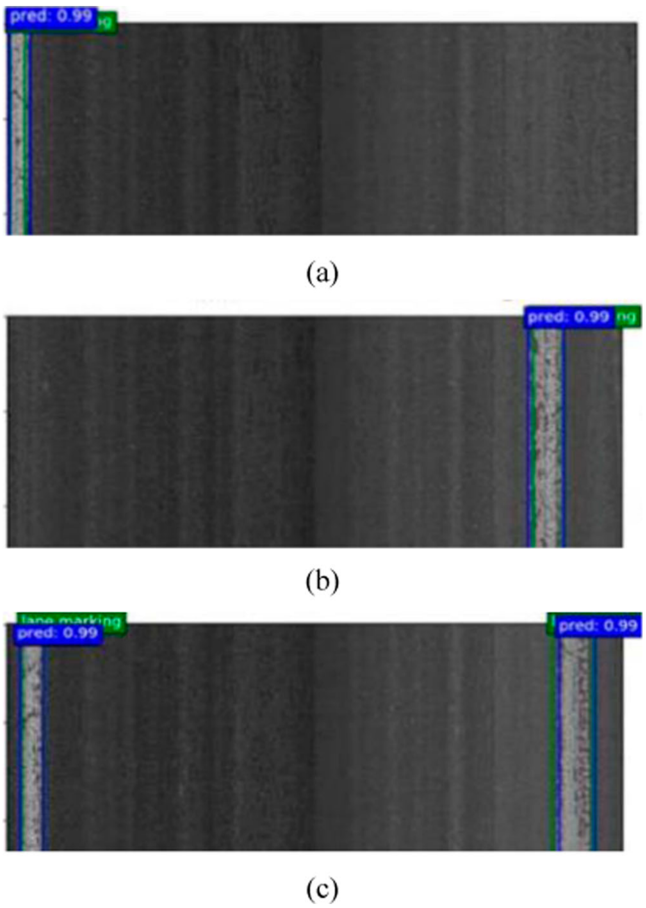

Figure 3. Identified lane markings based on the Faster R-CNN model: (a) pavement image with left lane marking; (b) pavement image with right lane marking; (c) pavement image with two-sides lane marking.

the test based on 4000 images, the precision is 0.9483, the recall is 0.9826 and the F value is 0.9651. The result shows that the Faster R-CNN presents excellent performance on lane marking identification.

4.1.2 Lateral distance from DHDV to pavement centre

Based on the detected lane markings, the lateral distance from pavement centre to DHDV's trajectory is measured. On two-lane highways the right lane marking is painted as a solid line, while the left lane marking (pavement centreline) is painted as a solid line on the no-overtaking sections and a dash line on the permitted overtaking sections. The large deviation of DHDV or the gap of dash lane marking would make none or only one lane marking captured on a pavement image. Three situations are analysed in this study.

(1) Left lane markings captured

If the captured left lane marking is straight and throughout an image, the lateral distance from DHDV to pavement centre is measured, as shown in Figure 4(a). If the captured left lane marking is presented as a slanted line, the lateral distance from the vehicle to the pavement centre is varied, as shown in Figure 4(b). If the captured left lane marking is not throughout an image, the gap is filled first, and then the lateral distance from the vehicle to the pavement centre is measured, as shown in Figure 4(c).

(2) Only the right lane marking captured

If the left lane marking (pavement centreline) is out of an image, the lane centreline is determined first based on the captured right lane marking and lane width. Subsequently, the lane offset of DHDV is measured, as shown in Figure 5. Finally, the lateral distance from DHDV to the pavement centre equals the half-lane width plus the lane offset.

(3) No lane marking captured

When no lane marking is captured in an image, the end points of lane markings on the last and the next images are marked and connected first, as shown in Figure 6. Subsequently, the missing part of the left lane marking on the current image is filled. Finally, the lateral distance from the DHDV to pavement centre (left lane marking) is measured, as shown in Figure 6.

4.1.3 Pavement centreline extraction

The heading angle measured by IMU is employed to plot DHDV's trajectory with the x – and the y-coordinate. The data collection frequency of IMU is 200 Hz. According to the 100 km/h speed of DHDV, the data collection interval is approximately 150 mm of IMU. A Gauss filter is used to eliminate the noise of raw heading angle data. The Distance Measurement Unit (DMI) installed on the rear wheel measures the moving distance of DHDV. Based on the measured moving distance and heading angles, the trajectory of DHDV is obtained. In Figure 7 T_i is the ith position on the vehicle's trajectory, and the x- and y-coordinate of T_i is obtained by referring to (1) and (2). Referring to the lateral distance from DHDV to the pavement centre, the trajectory of the pavement centreline is obtained. The data intervals are different for IMU (150 mm) and the 3D line scanning laser system (1 mm). For consistency, DHDV's trajectory is described with an interval of 150 mm. The left and right deviations from the pavement centreline are defined as a negative and a positive value, respectively. As shown in Figure 7, T'_i is the ith point on the pavement centreline trajectory. The x- and y-coordinate of T'_i are acquired by referring to (3) and (4), respectively.

$$x_i = D \times cosH_{i-1} \tag{1}$$

$$y_i = D \times sinH_{i-1} \tag{2}$$

$$x'_i = x_i + d_L \times sinH_i \tag{3}$$

$$\mathrm{T_i x'_i H_i y_i} y'_i = y_i - d_L \times cosH_i \tag{4}$$

wherex_i: the x-coordinate of T_i; y_i: the y-coordinate of T_i; D: the moving distance of two collection points of IMU; H_i: the heading angle of the ith position; x'_i: the x-coordinate of T'_i; y'_i: the y-coordinate of T'_i; d_L: the lateral deviation from DHDV to the pavement centreline.

4.2. Pavement horizontal alignment measurement

Based on the extracted trajectory of the pavement centreline the horizontal alignments of the roadway are measured, such

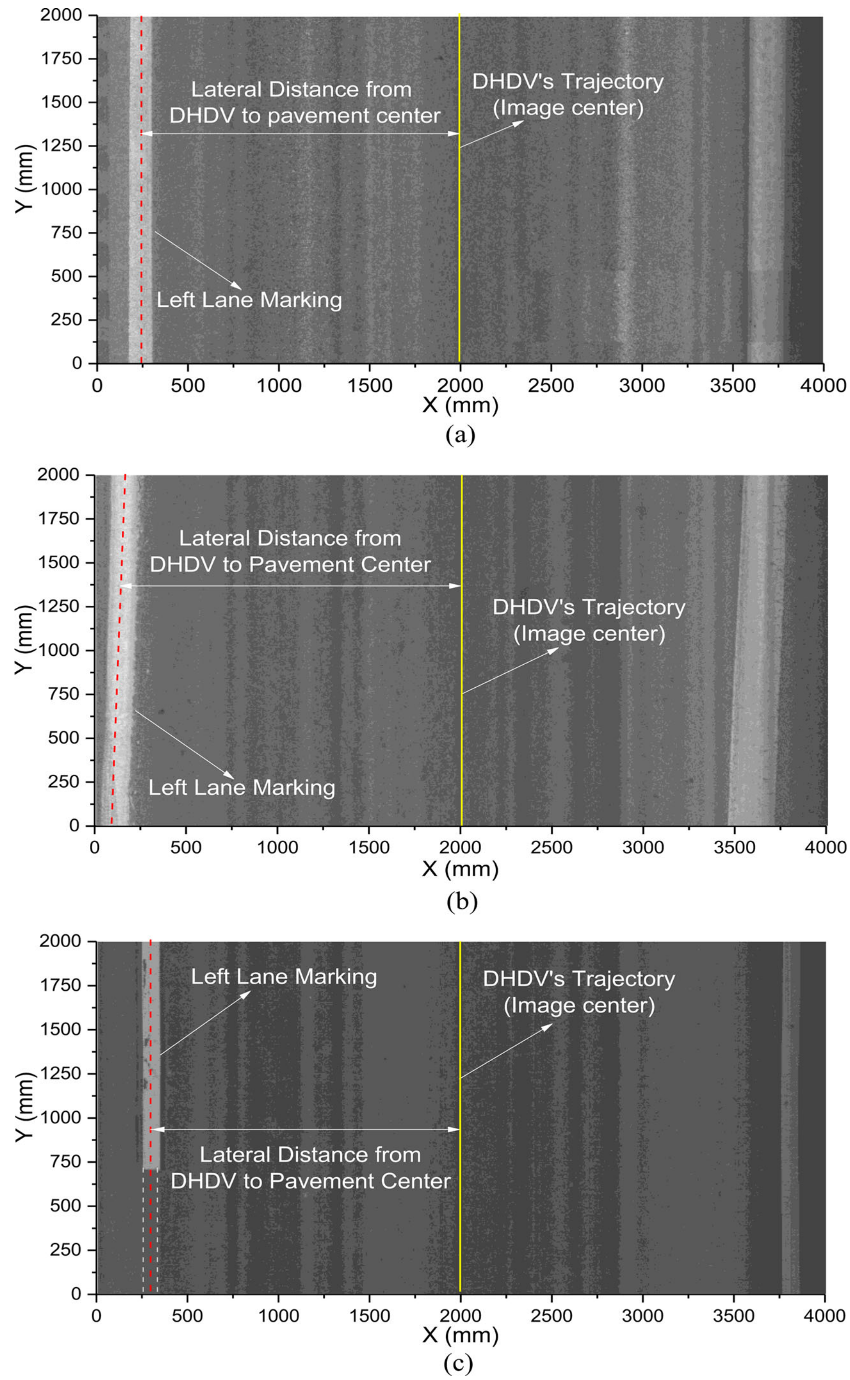

Figure 4. The lateral distance from the vehicle to the pavement centre for: (a) straight left markings; (b) slanted left markings; (c) defective left markings.

as Point of Curve (PC) station, Point of Tangent (PT) stations, curve radius and curve length.

4.2.1 PC and PT station identification

The heading angle of the pavement centreline is utilised to detect PC and PT stations. Generally, heading angles present as linear increases or decreases on the simple curvature, while it presents as a fixed value on tangent section. Based on this feature, the K-means clustering method is applied to detect the transition point of curved and tangent sections. Herein, K-value represents the quantity of curved or tangent sections. The second derivative of handing angles is calculated, and the number of their zero points is defined as K-value. Initial seed points (at random) are used for partitioning. The transition points of each cluster are defined as the PC/PT stations.

4.2.2 Horizontal alignment calculation

The Chord offset method is applied to calculate the curve radius in this study. First, two points on the curved section are selected randomly for curve radius calculation, as T'_j and T'_{j+n} are shown in Figure 8. Second, the midpoint between the two selected points is detected, as $T'_{j+(n/2)}$ shown in

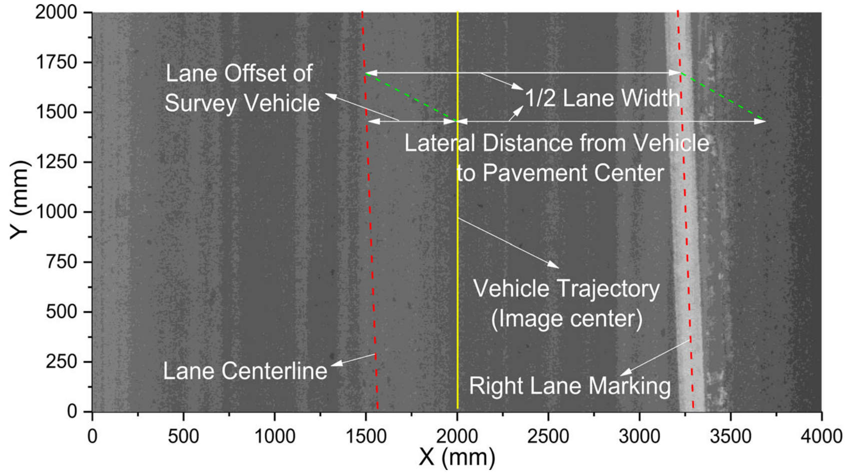

Figure 5. The lateral distance from the vehicle to the pavement centre for only the right lane marking captured

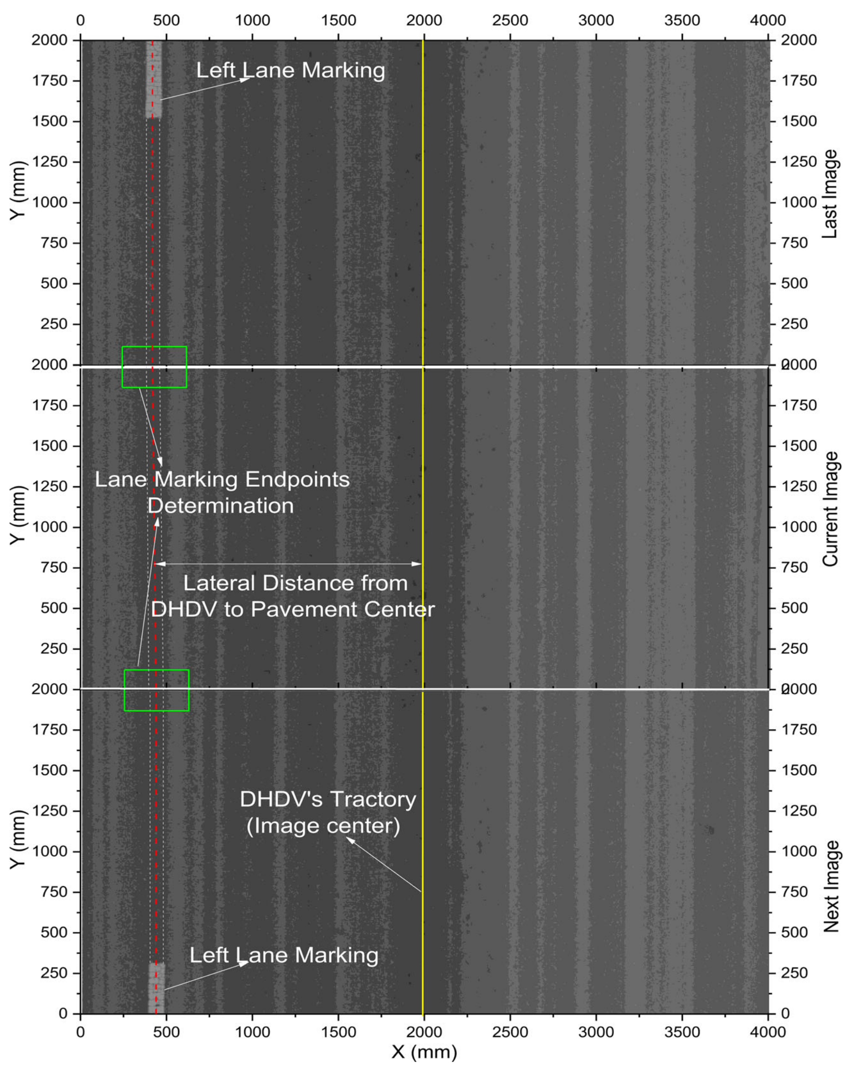

Figure 6. The lateral distance from the vehicle to the pavement centre for no lane marking captured.

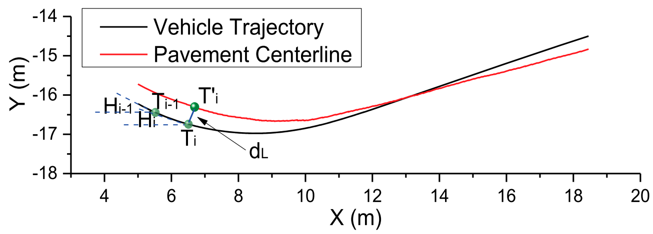

Figure 7. Pavement centreline trajectory acquisition.

Figure 8. The point 'O' is the curve centre. Finally, the curve radius is computed by referring to (5). Herein, 'L' is the linear distance between T'_j and T'_{j+n}, which is obtained by referring to (6); and the 'M' is the vertical distance from the point $T'_{j+(n/2)}$ to the linear line T'_j T'_{j+n} by referring to (7).

$$R = \frac{L^2}{8M} + \frac{M}{2} \tag{5}$$

$$L = \sqrt{(x'_{j+n} - x'_j)^2 + (y'_{j+n} - y'_j)^2} \tag{6}$$

$$M = \sqrt{\left(\frac{x'_{j+n} + x'_j}{2} - x'_{j+\frac{n}{2}}\right)^2 + \left(\frac{y'_{j+n} + y'_j}{2} - y'_{j+\frac{n}{2}}\right)^2} \tag{7}$$

where R: the curve radius of pavement centreline; L: the linear distance between T'_j and T'_{j+n}; M: the middle ordinate.

4.3. Pavement rutting trajectory extraction

The 3D laser images collected by the 3D line scanning laser system are full lane coverage, as shown in Figure 9. The longitudinal resolution of the 3D laser image is 1 mm. In other words, the 3D pavement image is composed of lane transverse profile data with 1 mm intervals. The lane transverse profile is utilised to extract the rutting trajectory.

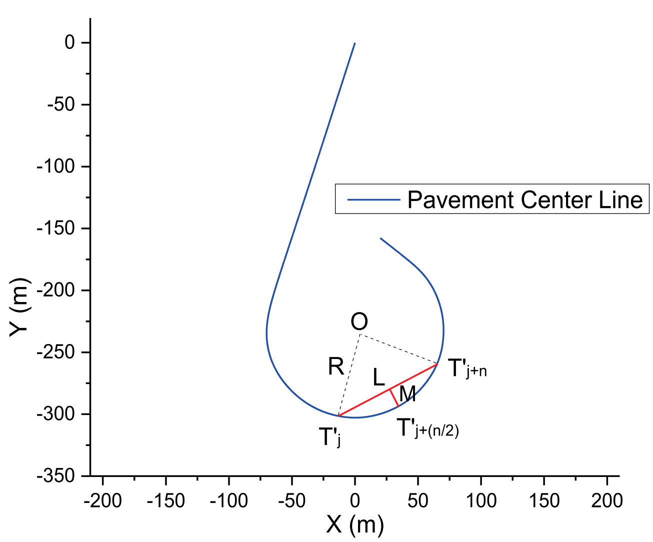

Figure 8. Curve radius measurement on pavement centreline.

4.3.1 Pavement rutting valley points search

The valley point is defined as the deepest point of left or right ruts on a transverse profile. The valley points of ruts are applied to describe rutting trajectories.

(1) Data smoothing

Due to the high vertical resolution of 3D laser data (0.3 mm) the pavement texture presents as waves on transverse profiling data, which is useless information for rutting measurement. Therefore, locally weighted regression scatter plot smoother (LOWESS) is applied to smooth the transverse profiling data.

(2) Undeformed axis determination

Repeated traffic load leads to pavement deformation. Undeformed pavement area is considered as the reference for depressed pavement area (pavement ruts) detection. The left and right edges of transverse profiling are utilised to determine the undeformed axis because wheel loads on that area appear in low frequency. The undeformed axis is established by linear fitting the inner and outer edges (100 mm in length) of the lane transverse profile, as shown in Figure 10.

(3) Valley point detection

To rebuild the lane transverse profile coinciding with the pavement in the real world, the lane transverse profile is rotated until its slope is consistent with the cross slope. Herein, the roll angle measured by IMU is defined as a cross slope. Subsequently, the locations of two-side lane markings on the transverse profile are marked by referring to the positions of lane markings on 2D images. The lane centre is determined based on the positions of lane markings, which are marked with orange colour in Figure 11. Referring to the undeformed axis, the points with maximum depth on the left and right section of the lane centre are defined as the valley points of the left and right ruts, as shown in Figure 11.

4.3.2 Pavement rutting lateral position measurement

The lateral position of a rut is described using the projection distance from the valley point to lane centre on the undeformed horizontal axis by referring to (8), as shown in Figure 11. The rutting centre is defined as the middle of two valley points, which is applied to measure the lane departure of rutting trajectories. The lane departure of rutting trajectories is calculated by referring to (9).

$$P_{Vi} = (x_{Vi} - x_{LC}) \times \sqrt{S_c^2 + 1} \tag{8}$$

$$DE_{ruts} = \left[\frac{1}{2}(x_{V1} + x_{V2}) - x_{LC}\right] \times \sqrt{S_c^2 + 1} \tag{9}$$

where P_{vi}: the lateral position of valley points on a lane ($i = 1$ for the left rut, $i = 2$ for the right rut); x_{LC}: the x-coordinate of lane centre line; S_c: pavement cross-slope; DE_{ruts}: the lane departure of ruts; x_{vi}: the x-coordinate of valley point ($i = 1$ for the left rut, $i = 2$ for the right rut).

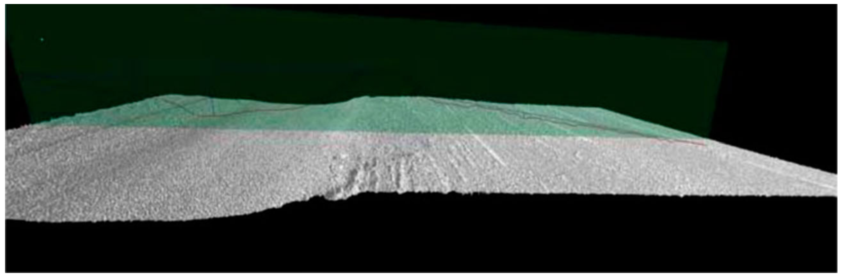

Figure 9. The example of 3D pavement rutting laser image.

5. Results and discussion

5.1. Test section

A road section of two-lane highways located in Arkansas U.S.A. is selected as the test section in this study, as shown in Figure 12. The test section is 8.776 km in length, and the limited speed is 112.65 km/h. The terrain of the selected test section slopes gently, so the influence of vertical alignments on lane departure can be ignored for the test site. The road condition of the test section is good. The maximum rutting depth of the test site is around 6 mm. Slight ruts would not make drivers follow the rutting trajectories, so the interference of ruts on vehicles' trajectories can be ignored for the test site.

5.2. Horizontal alignments of the test section

The locations of PC/PT stations, curve radius, turning direction of the curve and curve length of the test section are measured based on the proposed methods.

5.2.1. Trajectory of pavement centreline

The DHDV's trajectory in the eastbound test section is applied for pavement centreline extraction. The lateral distance from DHDV to the pavement centre is measured and shown in Figure 13. The trajectory of the pavement centreline is obtained by referring to DHDV's trajectory and its deviation from the pavement centre, as shown in Figure 14.

5.2.2. Horizontal alignments of curved ramps

The detected PC/PT stations, curved sections and turning directions of the test section are marked in Figure 14. There are a total of 18 curves in the test section. Among them eight are left turn curves, and ten are right turn curves for the eastbound. The turning direction of the curves on the westbound is contrary to that on the eastbound. The measured curve length, curve radius, turning direction and the locations of PC/PT stations are shown in Table 1.

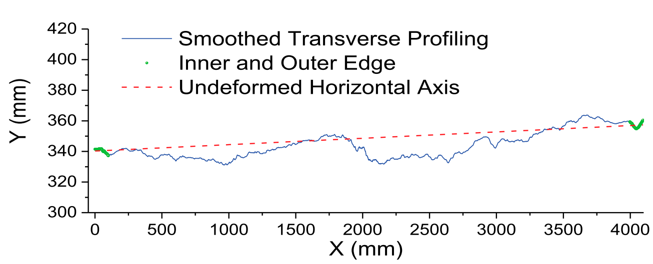

Figure 10. Establishing the undeformed axis of the pavement transverse profile.

5.2.3. Validation of measured horizontal alignments

A validation test was conducted in this study to verify the accuracy of measured horizontal alignments. The manual measurements of horizontal alignments are considered ground truth. To ensure the accuracy of the manual measurement, four engineers are selected to conduct manual measurements. Every engineer makes three measurements on each position. The maximum and the minimum results are removed, and the average value of the rest ten measurements is calculated and used to verify the automated measurement.

(1) Manual measurement

The manual measurement was conducted on the outside of the lane (outer lane marking), so traffic flow is not obstructed during the measurement. First, a straight scale is put on the tangent section of the outer lane marking. Subsequently, the straight scale keeps a parallel movement, until a bifurcation point appears between the straight scale and the outer lane marking. The bifurcation point is defined as a PC or PT station. Two pints on a curved section of outer lane marking are selected randomly for curve radius measurement. The crow flies between two selected points ('L') and the middle ordinate ('M') is manually measured. The curve radius of outer lane marking is calculated by the Chord Offset method by referring to (5), (6) and (7). Finally, it is transferred to the curve radius of the pavement centreline by adding lane width.

(2) Validation results

Five curves of the test section are selected for the validation test. The errors of automatic measurements are mathematically described by referring to (10) and (11). The validation results show that the average error on PC/PT detection is 2.04%, the average error on curve radius measurement is 6.25% and the average error on curve length measurement is 2.54%, as shown in Table 2. It implies that the proposed methods are robust in curve detection and curve radius measurement.

$$E_{PC/PT} = \frac{|D_{PC/PT}|}{L_{CM}} \tag{10}$$

$$E_R = \frac{|R_A - R_M|}{R_M} \tag{11}$$

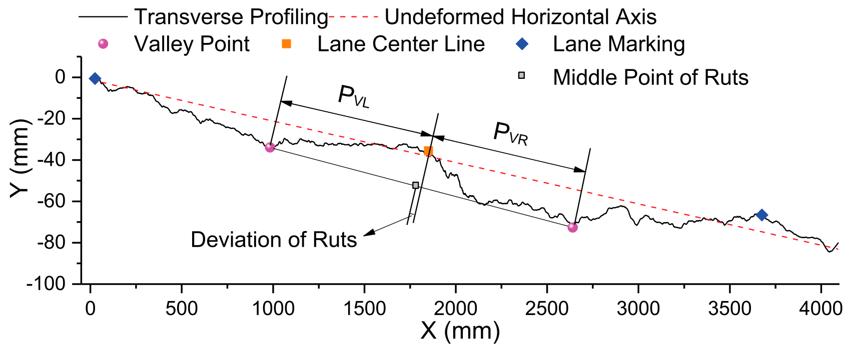

Figure 11. The lateral positions of the left and right ruts.

$$E_L = \frac{|L_{CM} - L_{CR}|}{L_{CR}} \tag{12}$$

where $E_{PC/PT}$: the errors on the PC/PT detection; $D_{PC/PT}$: the deviation of the automatically detected PC/PT locations from the ground truth; R_A: the automatically measured curve radius; R_M: the manually measured curve radius (ground truth); E_L: the errors on the curve length measurement by the presented method; L_{CR}: the manually measured curve length (ground truth); L_{CM}: the automatically measured curve length.

5.3. Pavement rutting trajectories of test sections

To compare the rutting trajectories on test sections of two opposite directions, the two datasets are matched by GPS coordinates, and their starting points are reset on the same location. In this study 1 m interval is applied to describe rutting trajectories.

5.3.1. Lateral position of lane markings on images

The lateral positions of lane markings on pavement images collected on the test site are shown in Figure 15, which are

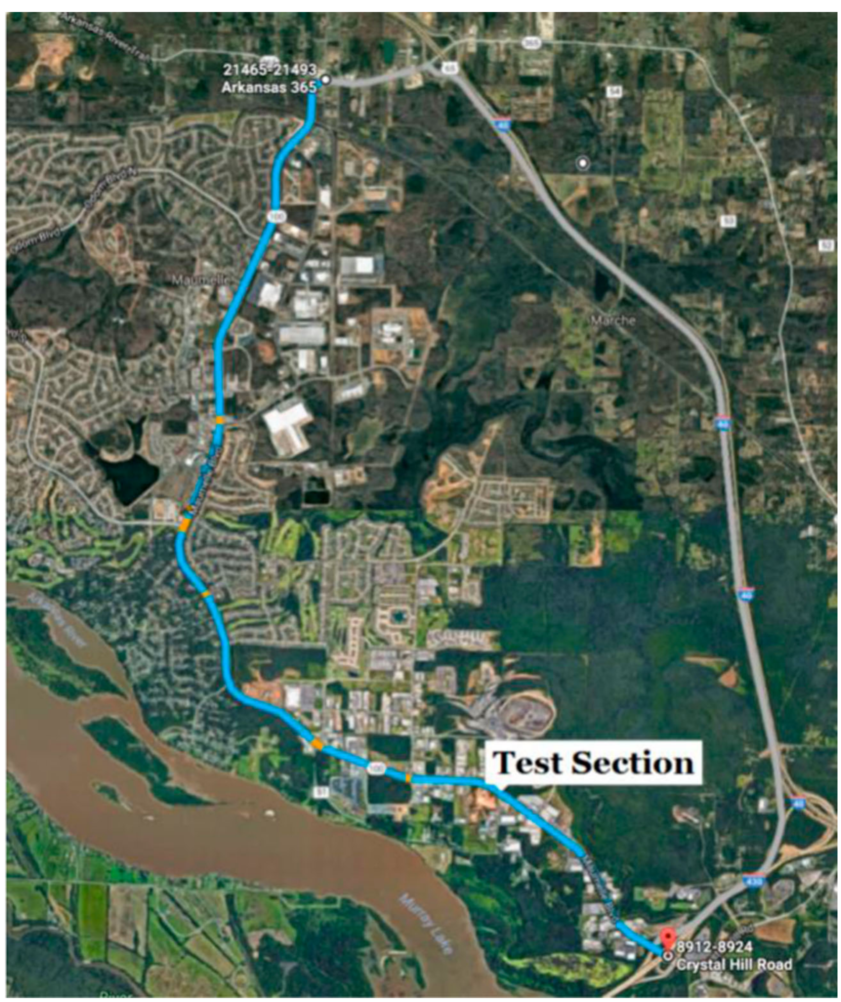

Figure 12. Test locations.

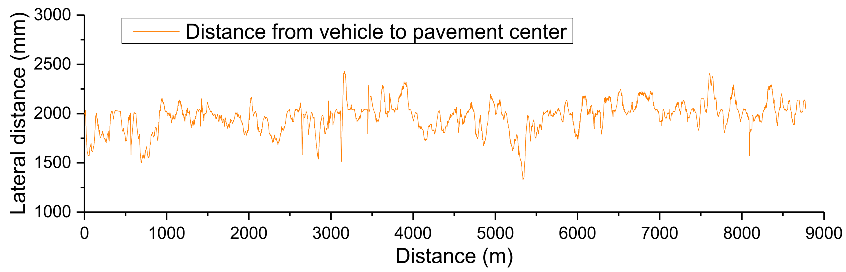

Figure 13. The lateral distance from DHDV to the pavement centre (East).

used to position pavement ruts. Due to the wheel wandering of DHDV, some lane markings are out of the shooting scope of cameras (4 m). The missing lane marking is filled by referring to lane width, and the lateral positions of them present as negative value or a value larger than 4000 mm, as shown in Figure 15.

5.3.2. Trajectories of the left and right ruts

Lane centreline is determined to refer to the detected lane markings, and it is used to describe the lateral positions of the left and right ruts. The left and right rutting trajectories on the test section of two opposite directions are shown in Figure 16. Herein, the red line represents lane centre, the positive value means the rut is located on the right side of lane centre, whereas the negative value means the rut is located on the left side of lane centre. The measured results show that the distance between the two valley points of the left and right ruts is not equal but has a large variation. Traffic flow includes different size vehicles, vehicle tilt and asymmetry load distribution of vehicles .

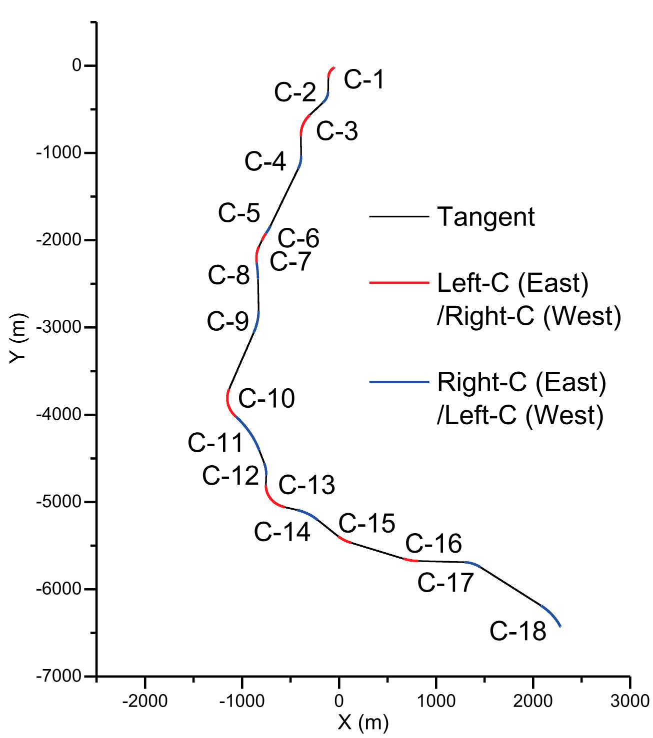

Figure 14. The detected curves on the pavement centreline trajectory.

5.3.3. Trajectory of two ruts centres

In this study rutting trajectories are applied to represent widespread vehicles' trajectories. The deviation of two rut centres from the lane centre is utilised to describe the regular pattern of lane departure. The positive deviation represents the rutting trajectories shifting to the right side of the lane centreline, whereas the negative deviation means the rutting trajectories shifting to the left side of the lane centreline, as shown in Figure 17.

5.3.4. Validation of measured rutting trajectory

The manual measurement of rutting lateral positions is conducted and considered as ground truth for validation tests. Similar to measure horizontal alignment, four engineers conduct manual measurement of the rutting position. Every engineer makes three measurements of the same position. The maximum and the minimum measured results are removed. The average value of the remaining ten

Table 1. The measured curves of the test section (Eastbound).

No.	PC (m)	PT (m)	Length (m)	R (m)	Turn Direct
C-1	0	136	136	135	Left
C-2	300	436	136	181	Right
C-3	634	900	266	331	Left
C-4	1126	1276	150	333	Right
C-5	1994	2088	94	454	Right
C-6	2088	2098	10	458	Left
C-7	2260	2450	190	339	Left
C-8	2450	2628	178	1486	Right
C-9	2998	3254	256	574	Right
C-10	3870	4294	424	294	Left
C-11	4294	4748	454	1033	Right
C-12	4906	5046	140	361	Right
C-13	5158	5504	346	258	Left
C-14	5638	5878	240	478	Right
C-15	6134	6316	182	298	Left
C-16	6886	7040	154	479	Left
C-17	7516	7692	176	300	Right
C-18	8456	8774	318	614	Right

Table 2. Validation results for curve measurement.

	PC/PT		Curve Length			Curve Radius		
No.	E_{PC} (%)	E_{PT} (%)	L_{CM} (m)	LCR (m)	EL (%)	RA (m)	RM (m)	ER (%)
C-2	1.57	2.67	136	138	−1.11	181	184	−1.51
C-4	1.83	4.83	150	146	3.01	333	347	−3.97
C-9	1.01	0.49	256	256	0.52	574	482	19.08
C-11	0.43	1.68	454	464	−2.12	1033	1052	−1.79
C-16	3.24	2.72	154	164	−5.97	479	504	−4.91
AE	2.04%		2.54%			6.25%		

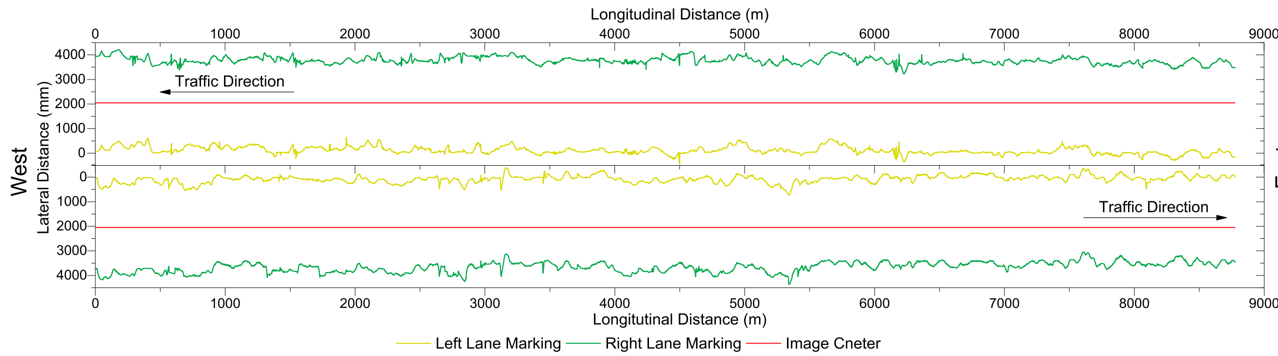

Figure 15. The lateral position of lane markings on pavement images.

measurements is calculated and applied to verify the automated measurement.

(1) Manual measurement

The manual measurement of rutting is conducted in the inner lane area. Therefore, obstructing traffic flow is needed to ensure the safety of surveyors. The resolution of the manual measurement is 1 cm based on the ability of human vision. First, a 2 m straight scale is put across the entire rut, and a 0.5 m straight needle perpendicular to the scale is applied to detect the valley point. The distance from the lane centreline to the valley point is measured and defined as the rutting lateral position.

(2) Validation results

A 100 m road segment of the test section is selected as the test bed for the validation test, and rutting measurement is conducted at 5 m intervals. To match the manual measurements, the automatic measurements in the same locations are extracted. The errors in automatic measurements of rutting lateral positions are mathematically described by referring to (13). The manual measurements and validation results are shown in Table 3. The average error on rutting lateral position measurement is 2.53%. It implies that the proposed automatic method is accurate in rutting lateral position measurement.

$$E_{RP} = \frac{|V_A - V_M|}{W_L} \tag{13}$$

where E_{RP}: the errors on the rutting position measurement; V_A: the automatically measured rutting position; V_M: the manually measured rutting position; W_L: the Lane width.

5.4. Lane departure detection for two-lane highways

Based on the strong relation between repeated wheel loads and pavement ruts, the deviation of pavement ruts from the lane centre is applied to detect lane departure in this study. The impactors of horizontal alignments on lane departure are analysed based on the data collected on two-lane highways. Indeed, the hazardous locations with lane departure are identified.

5.4.1. Impactors of horizontal alignments on lane departure

The test section is divided into several segments of curvatures and tangents, and the average lane departure (lane departure of ruts) of each segment is calculated and shown in Figure 18. Herein, the grey column represents the later deviation of widespread vehicles' trajectories from the lane centre. The positive deviations mean vehicles' trajectories shifting to the right of the lane centreline, whereas the negative deviations represent vehicles' trajectories shifting to the left of the lane centreline. The red line represents the curve radius of the test section. A zero value means the segment is tangent, a positive value means the segment is located on a right turn curve, and a negative value means the segment is located on aleft turn curve. The impacts of the undivided opposite lane, geometric feature,

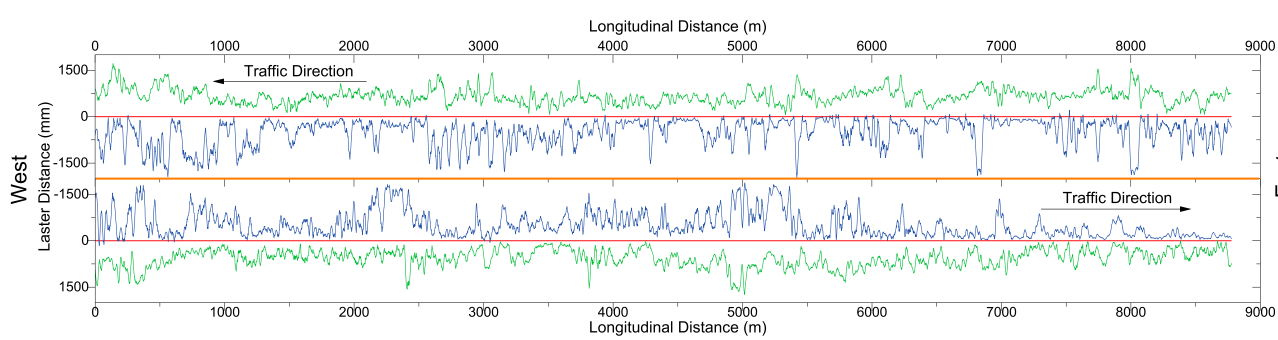

Figure 16. The left and right rutting trajectory on two opposing lanes of test sites.

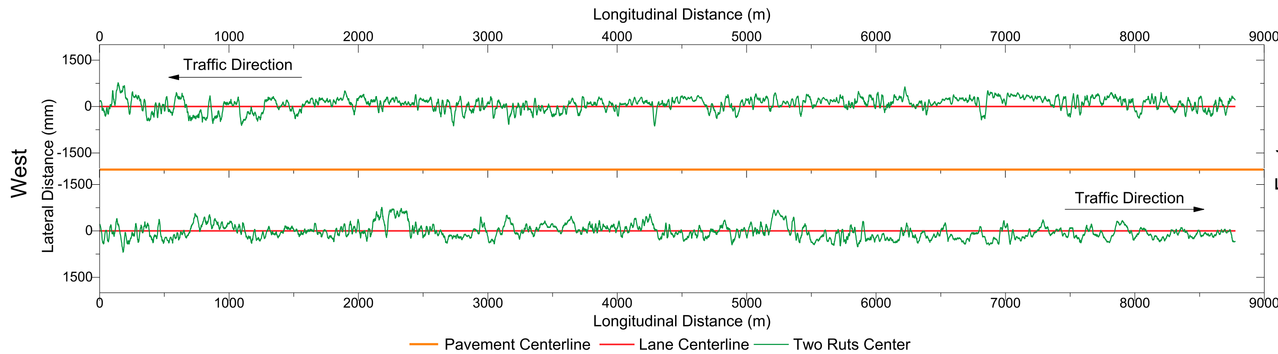

Figure 17. Automatically measured lane departure of rutting trajectories.

turning direction, curve radius and curve length on lane departure are analysed.

(1) Impacts of the undivided opposite lane on lane departure

The two lanes of two-lane highways have almost the same PC/PT stations and curve radius, but only the turning directions of curves are opposite. If there is no interference from the opposite traffic, the vehicles' trajectories on the eastbound and westbound lanes should have the same tendency and opposite deviation (inner or outer). In the real world, to avoid collision with opposite traffic, vehicles on both eastbound and westbound lanes prefer to shift to the outer side. The lengths of the road sections with the inner or outer deviation are counted and shown in Table 4. The results show that the outer lane departure occurs on almost 62.5% road section of the whole test site. It implies that the impact of opposite traffic is significant on vehicles' trajectories.

(2) Impacts of curve turning direction on lane departure

There are 18 curvatures on the test site. On the eastbound lane 8 are left turn curves, and 10 are right turn curves. Contrarily, on the westbound lane 10 are left turn curves, and 8 are right turn curves. The average lane departures of 18 left turn curves and 18 right turn curves are counted and shown in Table 5. The average lane departure on left turn curves is −29.84 mm (inner deviation), and the average lane departure on right turn curves is 83.33 mm (outer deviation). The statistical data imply that on two-lane highways the vehicles prefer to shift to the inner side on left turn curves while prefer to shift to the outer side on right turn curves. Generally, centrifugal force puts vehicles to the outside of the curve, whereas drivers prefer to drag the vehicles back. The result of the struggle between the centrifugal force and drivers' behaviours decides the deviation of vehicles in inner or outer sides. The field data illustrate the impact of drivers' behaviours is greater than that of centrifugal force for the two-lane highways.

(3) Impacts of the geometric feature on lane departure

There are a total of 15 tangents and 18 curvatures on the test site. The average lane departures on tangents and curves are counted and shown in Table 5. Based on the field data, the average lane departure is 70.27 mm (outer deviation) on tangent sections −29.84 mm (inner deviation) on left turn curves, and 83.33 mm (outer deviation) on right turn curves. It is

Table 3. Validation results for rutting positioning.

	Left Rut Position (East)			Right Rut Position (East)			Left Rut Position (West)			Right Rut Position (West)		
Distance (m)	VA (mm)	VM (mm)	ERP (%)	VA (mm)	VM (mm)	ERP (%)	VA (mm)	VM (mm)	ERP (%)	VA (mm)	VM (mm)	ERP (%)
900	−342	−380	1.01	1262	1350	2.35	−1506	−1420	2.29	600	490	2.93
905	−1070	−890	4.80	230	160	1.87	−1456	−1540	2.24	604	740	3.63
910	−1038	−1200	4.32	626	790	4.37	−1496	−1380	3.09	152	266	3.04
915	−552	−690	3.68	162	330	4.48	−1514	−1660	3.89	508	750	6.45
920	−982	−1110	3.41	258	350	2.45	−154	−250	2.56	1654	1510	3.84
925	−996	−1020	0.64	1014	1120	2.83	−152	−190	1.01	544	490	1.44
930	−1166	−960	5.49	170	160	0.27	−1760	−1810	1.33	400	520	3.20
935	−256	−350	2.51	420	390	0.80	−1648	−1640	0.21	176	190	0.37
940	−1066	−980	2.29	196	340	3.84	−1704	−1660	1.17	412	390	0.59
945	−812	−1020	5.55	1364	1450	2.29	−1692	−1720	0.75	342	490	3.95
950	−562	−430	3.52	786	880	2.51	−1688	−1750	1.65	302	520	5.81
955	−362	−460	2.61	255	190	1.73	−156	−230	1.97	476	570	2.51
960	−736	−630	2.83	166	240	1.97	−294	−180	3.04	200	170	0.80
965	−1106	−1260	4.11	174	330	4.16	−112	−260	3.95	406	320	2.29
970	−384	−430	1.23	116	210	2.51	−220	−350	3.47	262	350	2.35
975	−190	−220	0.80	156	260	2.77	−302	−250	1.39	352	410	1.55
980	−212	−190	0.59	184	150	0.91	−320	−260	1.60	1796	1520	7.36
985	−306	−250	1.49	404	380	0.64	−308	−350	1.12	288	360	1.92
990	−838	−990	4.05	384	290	2.51	−1824	−1740	2.24	150	220	1.87
995	−958	−1110	4.05	268	170	2.61	−129	−210	2.16	590	640	1.33
1000	−346	−430	2.24	170	130	1.07	−514	−460	1.44	224	330	2.83
Average ERP		2.92%			2.33%			2.03%			2.86%	

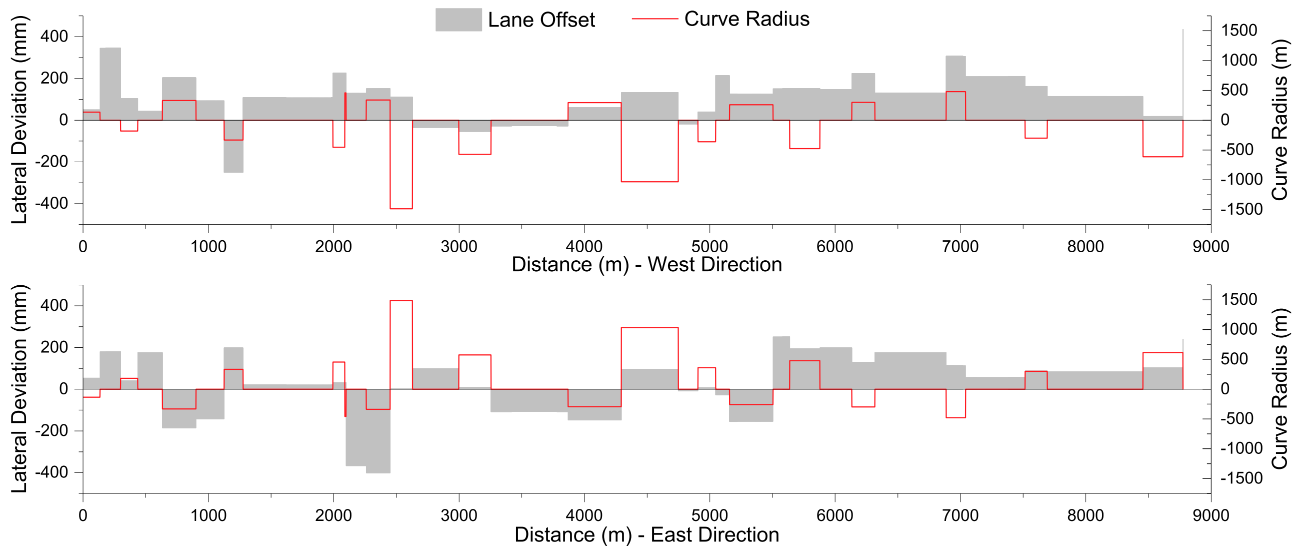

Figure 18. Segment statistics of lane departure based on horizontal alignments.

mentioned above that vehicles prefer to shift to the inner side of the road on left turn curves, while prefer to shift to the outer side of the road on right turn curves. Differently, there is no centrifugal force and unwanted turning operation on tangent sections, so the deviation of vehicles on the tangent section would be small. Therefore, compared with the vehicles' trajectories on the left and right turn curves, the vehicles' trajectories on tangent sections seem to locate in the middle of them. On two-lane highways the impact of horizontal alignments on lane departure is small on tangents, but the impact of opposite traffic on lane departure is still significant on tangents. It is concluded that on the tangent section of two-lane highway vehicles prefer to shift to the outer side of the road to avoid collision with opposite traffic.

(4) Impacts of curve radius on lane departure

To investigate the impacts of curve radius on lane departure, the curves are classified into five categories by their radius, as shown in Table 6. The average lane departure on each category of curves is counted. On left turn curves vehicles prefer to shift to the inner side of the road when the curve radius is smaller than 400 m, and the lane departure reaches the maximum value on the curves with a radius from 301 to 400 m. However, vehicles prefer to shift to the outer side of the road when the curve radius is larger than 400 m, and the lane departure decreases with the continuous increase of the curve radius. Different from left turn curves, vehicles prefer to shift to the outer side of the road. With the increase of curve radius the lane departure increases. However, when the curve radius is larger than 500 m, the lane departure decreases. The field data show on two-lane highways the curved sections with radius ranging from 300 to 500 m have larger lane departure than other curved sections.

(5) Impacts of curve length on lane departure

Based on the curve length of the test site, the curves are classified into three groups. The average lane departure on each group of curved sections is counted, as shown in Table 7. For right turn curves the turning operation and opposite traffic have the same effect of making vehicles shift to the outer side. The turning operation continues more times on the long curvature. Therefore, on the right turn curves the outer lane departure increases with the increase in curve length. However, for left turn curves the turning operation makes vehicles shift to the inner side, but opposite traffic

Table 4. Section length with the inner or outer lane departure.

Traffic Direction	Inner or Outer Lane Departure	Section Length (m)
East	Inner	3732
	Outer	5023
West	Inner	2847
	Outer	5916

Table 5. Average lane departure on tangent and curvatures.

Horizontal Alignment	Average Lane Departure (mm)
Tangent	70.27
Left Turn Curve	−29.84
Right Turn Curve	83.33

Table 6. Average lane departure of curves with different radii.

	Average Lane Departure (mm)	
Curve Radius (m)	Left-Turn Curve	Right-Turn Curve
100∼200	−25.48	46.26
201∼300	−57.37	112.31
301∼400	−212.35	153.83
401∼500	159.03	195.17
>500	59.78	65.50

Table 7. Average lane departure of curves with different lengths.

	Average Lane Departure (mm)	
Curve Length (m)	Left-Turn Curve	Right-Turn Curve
0∼150	−21.92	70.06
151∼300	−7.75	77.85
>300	−33.35	95.16

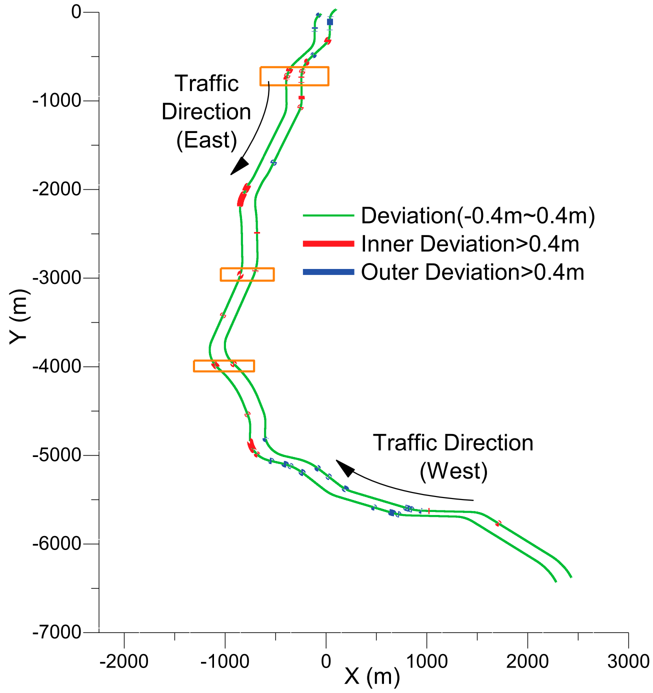

Figure 19. The detected lane departure of the test section.

makes vehicles shift to the outer side. Although the turning operation continues more times on the long curvature, the effects of opposite traffic also increase. Under the comprehensive effects of turning operation and opposite traffic, for left turn curves the lane departure is smaller on the type of curvatures with length ranging from 151 to 300 m than other types of curvatures. The statistical results show the impact of curve length is significant for two-lane highways.

5.4.2. Hazardous location with lane departure

The outer deviation may cause vehicles out of the lane, and the inner deviation may lead to a collision. According to the lane width (3.65 m) and vehicles' width (ranging from 1.8 to 2.3 m), 0.4 m is used to define the levels of lane departure. A deviation smaller than or equal to 0.4 m is considered with small lane departure. A deviation larger than 0.4 m is considered with large lane departure. The road sections having large lane departure with the inner and outer deviations are marked in Figure 19 with a red line and a blue line, respectively.

As shown in Figure 19, most of the red lines (high risk of the inner deviation) are located on the left turn curves of the test site; most of the blue lines are located on the transition sections of curves and tangents. The inner deviation on the undivided lanes with opposite traffic may cause a collision that is more serious accidents than the accidents caused by outer deviation. Especially, on curve 3, curve 9, and curve 10 the vehicles' trajectories of both westbound and eastbound roads shift to the inner side. These road sections have the highest risk of collision, which is marked in Figure 19. Curve 6, curve 7 and curve 13 of eastbound are the left turn curve with a radius from 300 to 400 m, and also the inner lane departure occurs in that area. However, these locations have lower risk than the marked area of Figure 19, because there is no deviation or outer deviation on the curves on the westbound. There are relatively more inward offsets on the eastbound lane than that on the westbound lane. The reason is that the features of the curves on the eastbound lane, including turning direction, curve radius and curve length, have a stronger effect of making vehicles with inward offset.

6. Conclusions

In view of the strong relationship between the trajectories of vehicles and pavement ruts, this paper proposes a method to detect lane departure and identify hazardous locations based on rutting trajectories. A test site of two-lane highways in the U.S. is chosen for the case study, and based on the collected data the impacts of horizontal alignments on lane departure are analysed. The conclusions are as follows.

The horizontal alignments including curve radius, curve length and PC/PT stations are automatically measured by the proposed method. The manual measurement of PC/PT stations and curve radius is considered ground truth to validate the automatic measurements. The average error is 2.04% on PC/PT detection, 2.54% on curve length measurement and 6.25% on curve radius measurement, which illustrates the proposed methods are robust in horizontal alignment measurement.

The rutting trajectories are extracted based on the proposed method and the continually collected transverse profile. The manual measurements of the rutting lateral position are considered ground truth for the validation test. The average error is 2.53%, which implies that the proposed method is accurate in rutting trajectories measurement.

The impacts of horizontal alignments including undivided opposite lane, curve turning direction, geometric feature, curve radius and curve length on lane departure are analysed based on the data collected on the test site of two-lane highways. The statistical data collected on two-lane highways show that most vehicles prefer to shift to the outer side on tangents and right-turn curves to avoid collision with opposite traffic; left-turn curves have a high risk of collision because vehicles prefer to shift to the inner side on left-turn curves; the road sections with curve radius ranging from 300 to 500 m have large lane departure; and general with an increase of curve length lane departure increases. The hazardous locations with lane departure are identified for the test site of two-lane highways. The identified result shows some of the left-turn curves are high-risk areas of collision. In future research, we will connect with the traffic police department to get the crash data on test sites. Then, we will compare the identified high-risk area and the actual driver's risk perception to verify the measurement detection.

This study provides a novel, accurate and automatic method to detect lane departure of the roadway. The proposed method is embedded into the software for data processing of the 3D line scanning system. Based on this software, the results for detecting hazardous locations with potential lane departure risk are automated outputted after the road survey. It archives automatic and fast data processing, so it makes the application simpler and quicker. Two-lane highways have a higher risk of collision, so they are selected as the test bed in this study. The measured horizontal alignments and rutting trajectories are helpful for traffic safety analysis of two-lane highways. Pavement engineers may take remedial measures, such as posting warning signs about wheel wandering to minimise traffic accidents on two-lane highways. In future research the provided methods will be applied to lane departure detection of other types of multiple-lane roads.

Disclosure statement

No potential conflict of interest was reported by the author(s).

Funding

This work was supported by University Industry Cooperation Project in Fujian China: [grant number 2020H6009]; National Key R&D Program of China [grant number 2021YFB3202901]; State Key Laboratory of Rail Traffic Control and Safety China: [grant number RCS2020K004].

ORCID

Wenting Luo http://orcid.org/0000-0001-5585-8467

References

Ai, C., and Tsai, Y., 2014. Automatic horizontal curve identification and measurement method using GPS data. *Journal of Transportation Engineering*, 141 (2), 04014078. DOI: 10.1061/(ASCE)TE.1943-5436.0000740.

Ben-Arieh, D., *et al.*, 2004. Geometric modeling of highways using global positioning system data and B-Spline approximation. *Journal of Transportation Engineering*, 130 (5), 632–636. DOI: 10.1061/(ASCE)0733-947X(2004)130:5(632).

Bento, L. C., Bonnifait, P., and Nunes, U. J., 2019. Set-membership position estimation with GNSS pseudorange error mitigation using lane-boundary measurements. *IEEE Transactions on Intelligent Transportation Systems*, 20 (1), 185–194. DOI: 10.1109/TITS.2018.2808542.

Bosurgi, G., *et al.*, 2022. An automatic pothole detection algorithm using pavement 3D data. *International Journal of Pavement Engineering*, in press, DOI: 10.1080/10298436.2022.2057978.

Choi, S. Y., and Lee, J. M., 2006. Applications of moving windows technique to autonomous vehicle navigation. *Image and Vision Computing*, 24 (2), 120–130. DOI: 10.1016/j.imavis.2005.09.016.

Deng, Z., *et al.*, 2017. Toward fast and accurate vehicle detection in aerial images using coupled region-based convolutional neural networks. *IEEE Journal of Selected Topics in Applied Earth Observations and Remote Sensing*, 10 (8), 3652–3664. DOI: 10.1109/JSTARS.2017.2694890.

Ding, S., *et al.*, 2022. 3D imaging based pavement texture evaluation. *International Journal of Pavement Engineering*, in press, DOI: 10.1080/10298436.2022.2077942.

Ekblad, J., *et al.*, 2021. Impact on rutting from introduction of increased axle loads in Finland. *International Journal of Pavement Engineering*, 22 (13), 1731–1743. DOI: 10.1080/10298436.2020.1721497.

Findley, D. J., Cunningham, C. M., and Hummer, J. E., 2011. Comparison of mobile and manual data collection for roadway components. *Transportation Research Part C: Emerging Technology*, 19 (3), 521–540. DOI: 10.1016/j.trc.2010.08.002.

Gao, R., *et al.*, 2021. Small foreign metal objects detection in X-Ray images of clothing products using faster R-CNN and feature pyramid network. *IEEE Transactions on Instrumentation and Measurement*, 70, 1–11. DOI: 10.1109/TIM.2021.3077666.

Gungor, O.E., and Al-Qadi, I.L., 2022. Wander 2D: a flexible pavement design framework for autonomous and connected trucks. *International Journal of Pavement Engineering*, 23 (1), 121–136. DOI: 10.1080/10298436.2020.1735636.

Hanley, P. F., and Forkenbrock, D. J., 2005. Safety of passing longer combination vehicles on two-lane highways. *Transportation Research Part A: Policy and Practice*, 39 (1), 1–15. DOI: 10.1016/j.tra.2004.09.001.

Hong, Z., *et al.*, 2018. Line-laser-based visual measurement for pavement 3D rut depth in driving state. *Electronics Letters*, 54 (20), 1172–1173. DOI: 10.1049/el.2018.5437.

Hong, Z., Ai, Q., and Chen, K., 2018. Line-laser-based visual measurement for pavement 3D rut depth in driving state. *Electronics Letters*, 54 (20), 1172–1173. DOI: 10.1049/el.2018.5437.

Hui, B., *et al.*, 2018. Critical assessment of the impact of vehicle wandering on rut depth measurement accuracy using 13-point based lasers. *Measurement*, 123, 246–253. DOI: 10.1016/j.measurement.2018.03.069.

Imran, M., Hssan, Y. M., and Patterson, D., 2006. GPS-GIS-based procedure for tracking vehicle path on horizontal alignments. *Computer-Aided Civil and Infrastructure Engineering*, 12 (5), 383–394. DOI: 10.1111/j.1467-8667.2006.00444.x.

Ishikawa, K., *et al.*, 2007. A mobile mapping system for precise road line localization using a single camera and 3D road model. *Journal of Robotics and Mechatronics*, 19 (2), 174–180. DOI: 10.20965/jrm.2007.p0174.

Kim, W., *et al.*, 2018. Vehicle path prediction using yaw acceleration for adaptive cruise control. *IEEE Transactions on Intelligent Transportation Systems*, 19 (12), 3818–3829. DOI: 10.1109/TITS.2018.2789482.

Li, L., Luo, W., and Wang, K. C. P., 2018. Lane marking detection and reconstruction with line-scan imaging data. *Sensors*, 18 (5), 1635. DOI: 10.3390/s18051635.

Luo, W., and Li, L., 2018. Automatic geometry measurement for curved ramps using inertial measurement unit and 3D LiDAR system. *Automation in Construction*, 94, 214–232. DOI: 10.1016/j.autcon.2018.07.004.

Luo, W., Li, L., and Wang, K. C.P., 2018. Automatic horizontal curve identification and measurement using mobile mapping systems (MMS). *Journal of Surveying Engineering*, 144 (4), 04018007. DOI: 10.1061/(ASCE)SU.1943-5428.0000257.

Luo, W., Liu, L., and Li, L., 2020. Measuring rutting dimension and lateral position using 3D line scanning laser and inertial measuring unit. *Automation in Construction*, 111, 103056. DOI: 10.1016/j.autcon.2019.103056.

Luo, W., Wang, K. C.P., and Li, L., 2019. Estimation of water film depth for rutting pavement using IMU and 3D laser imaging data. *International Journal of Pavement Engineering*, 20 (10), 1170–1181. DOI: 10.1080/10298436.2017.1394099.

Outay, F., Mengash, H. a., and Adnan, M., 2020. Applications of unmanned aerial vehicle (UAV) in road safety, traffic and highway infrastructure management: recent advances and challenges. *Transportation Research Part A: Policy and Practice*, 141, 116–129. DOI: 10.1016/j.tra.2020.09.018.

Qiu, S., *et al.*, 2018. A comprehensive system for AASHTO PP69-10-based pavement rut evaluation using 1-mm 3D pavement surface model. *International Journal of Pavement Engineering*, 19 (6), 489–501. DOI: 10.1080/10298436.2016.1176163.

Rasdorf, W., *et al.*, 2012. Evaluation of GIS applications for horizontal curve data collection. *Journal of Computing in Civil Engineering*, 26 (2), 191–203. DOI: 10.1061/(ASCE)CP.1943-5487.0000127.

Saleeb, A., *et al.*, 2005. Numerical simulation techniques for HMA rutting under loaded wheel tester. *International Journal of Pavement Engineering*, 6 (1), 57–66. DOI: 10.1080/10298430500068704.

Saleh, M., 2020. Modified wheel tracker as a potential replacement for the current conventional wheel trackers. *International Journal of Pavement Engineering*, 21 (1), 20–28. DOI: 10.1080/10298436.2018.1435880.

Siddharthan, R.V., *et al.*, 2017. Investigation of impact of wheel wander on pavement performance. *Road Materials and Pavement Design*, 18 (2), 390–407. DOI: 10.1080/14680629.2016.1162730.

Tsai, Y., Wu, J., and Wang, Z., 2010. Horizontal roadway curvature computation algorithm using vision technology. *Computer-Aided Civil and Infrastructure Engineering*, 25 (2), 78–88. DOI: 10.1111/j.1467-8667.2009.00622.x.

Yeganeh, A., Vandoren, B., and Pirdavani, A., 2021. Impacts of load distribution and lane width on pavement rutting performance for automated vehicles. *International Journal of Pavement Engineering*, in press, DOI: 10.1080/10298436.2021.1935938.

Yeganeh, A., Vandoren, B., and Pirdavani, A., 2022. Pavement rutting performance analysis of automated vehicles: impacts of wander mode, lane width, and market penetration rate. *International Journal of Pavement Engineering*, in press, DOI: 10.1080/10298436.2022.2049264.

Zhai, Y., *et al.*, 2021. Hybrid knowledge R-CNN for transmission line multifitting detection. *IEEE Transactions on Instrumentation and Measurement*, 70, 1–12. DOI: 10.1109/TIM.2021.3096600.

Zhang, D., *et al.*, 2018. Automatic pavement defect detection using 3D laser profiling technology. *Automation in Construction*, 96, 350–365. DOI: 10.1016/j.autcon.2018.09.019.

Zhang, J., *et al.*, 2018. Terahertz image detection with the improved faster region-based convolutional neural network. *Sensors*, 18 (7), 2327. DOI: 10.3390/s18072327.

Zhang, K., Zhang, Z., and Luo, Y., 2018. Inspection method and evaluation standard based on cylindrical core sample for rutting resistance of asphalt pavement. *Measurement*, 117, 241–251. DOI: 10.1016/j.measurement.2017.12.002.

Zhao, Z., *et al.*, 2020. Factors affecting the rutting resistance of asphalt pavement based on the field cores using multi-sequenced repeated loading test. *Construction and Building Materials*, 253, 0950–0618. DOI: 10.1016/j.conbuildmat.2020.118902.

Zhou, F., *et al.*, 2019. Optimization of lateral wandering of automated vehicles to reduce hydroplaning potential and to improve pavement life. *Transportation Research Record*, 2673, 81–89. DOI: 10.1177/0361198119853560.